

GaN-Based Deep-Nano Structures: Break the Efficiency Bottleneck of Conventional Nanoscale Optoelectronics

Ishtiaque Ahmed Navid, Ayush Pandey, Yin Min Goh, Jonathan Schwartz, Robert Hovden, and Zetian Mi*

Conventional semiconducting nanowire optoelectronic devices generally exhibit low efficiency, due to dominant nonradiative surface recombination. Here, it is shown that such a critical challenge can be potentially addressed by exploiting semiconducting structures in the deep-nanoregime. The epitaxy and structural and optical characteristics of GaN-based micro-network nanostructures grown on Si wafer are studied. These complex nanostructures have lateral dimensions as small as a few nanometers. Detailed scanning transmission electron microscopy studies suggest that the self-assembled micro-network nanostructures are monocrystalline, despite the porous nature. Significantly, such micro-network nanostructures exhibit ultrabright emission in the visible spectrum. Compared to conventional InGaN nanowire structures with similar surface area, the surface recombination velocity of such deep-nanostructures is reduced by nearly two orders of magnitude, which is evidenced by the extremely bright luminescence emission as well as the long carrier lifetime measured under low excitation conditions. This study offers a new path for the design and development of next generation high efficiency nanoscale optoelectronic devices.

1. Introduction

In the past two decades, semiconducting nanostructures, e.g., nanowires, have been extensively studied for applications in optoelectronics, including LEDs, lasers, solar cells, and photodetectors.^[1] To date, however, it has remained a daunting challenge to achieve high efficiency nanoscale optoelectronic devices. It is generally believed that the underlying challenge is directly related to the enhanced nonradiative surface recombination, due to the large surface area.^[2] As an example, while broad area InGaN blue quantum well LEDs can exhibit external


quantum efficiency (EQE) >80%,^[3] the efficiency decreases by at least one to two orders of magnitude when the device dimensions are reduced to micrometer, or nanoscale, due to the dominant nonradiative surface recombination.^[4] The *efficiency cliff* of optoelectronics, i.e., drastically reduced efficiency when the device sizes are shrunk to the micro or nanoscale, becomes even more severe for III-nitride light emitters in the deep visible (green to red), due to the large lattice mismatch ($\approx 11\%$) between GaN and InN,^[5] which not only leads to the formation of extensive defects, disorders, and dislocations but also significantly reduces the electron–hole wavefunction overlap due to piezoelectric field induced polarization.^[6]

The commonly reported semiconducting nanowires for applications in optoelectronics have lateral dimensions on the order of 100 nm or larger. Glas et al.^[7] analyzed the critical dimensions for the plastic

relaxation of semiconducting nanowires, showing that the critical layer thickness depends strongly on the nanowire diameter. Schematically shown in **Figure 1** is the estimated critical layer thickness plotted versus the nanowire diameter for a heterostructure with lattice mismatch $\approx 4\%$, corresponding approximately to $\text{In}_{0.32}\text{Ga}_{0.68}\text{N}$ grown on GaN emitting in the green spectrum. The critical layer thickness is ≈ 1 nm for conventional planar heterostructures (shaded gray region in Figure 1), which is increased to ≈ 3 nm for InGaN nanowire structures with diameters ≈ 100 nm (shaded blue region in Figure 1). It is therefore seen that the epitaxy of conventional InGaN/GaN nanowire arrays inevitably leads to certain level of defect formation. The resulting dominant nonradiative (surface) recombination is evident by the extremely short carrier lifetime (sub nanosecond) commonly measured for nanowire structures at room temperature,^[8] compared to a few nanoseconds of their planar counterparts, which explains largely the low efficiency of conventional nanowire optoelectronic devices.^[9] The critical layer thickness, however, can be potentially increased to an indefinitely large value if the lateral dimensions are further reduced to the deep-nano regime (< 40 nm), shown as the shaded green region in Figure 1. Indeed, recent studies suggested that strain relaxation was most efficient in InGaN/GaN nanostructures with lateral dimensions < 40 nm,^[10] consistent with the calculation by Glas et al.^[7] Efficient strain relaxation of InGaN

I. A. Navid, A. Pandey, Z. Mi
Department of Electrical Engineering and Computer Science
University of Michigan
Ann Arbor
1301 Beal Avenue, Ann Arbor, MI 48109, USA
E-mail: ztmi@umich.edu

Y. M. Goh, J. Schwartz, R. Hovden
Department of Materials Science and Engineering
University of Michigan, Ann Arbor
2300 Hayward St, Ann Arbor, MI 48109, USA

 The ORCID identification number(s) for the author(s) of this article can be found under <https://doi.org/10.1002/adom.202102263>.

DOI: 10.1002/adom.202102263

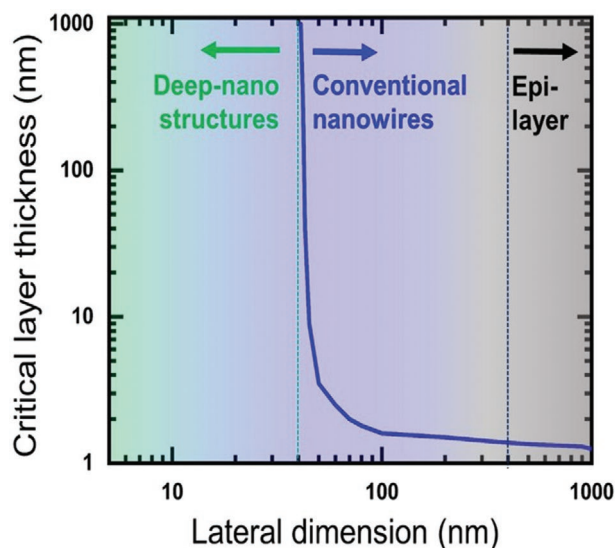


Figure 1. Schematic illustration of the critical thickness variation of a lattice-mismatched heterostructure as a function of the lateral dimension. Blue curve: Variation of the critical layer thickness for a misfitting layer (misfit $\approx 4\%$) growing on top of a nanowire as a function of the nanowire radius (adapted from Glas et al.^[7]). It is seen that in the deep-nano regime, the critical layer thickness can be infinitely large.

nanostructures not only drastically reduces defect densities but also significantly enhances the exciton binding energy due to the increased electron–hole wavefunction overlap.^[6c] A nearly 100-fold enhancement in the exciton oscillator strength was measured in InGaN nanostructures with lateral dimensions < 40 nm.^[10b] It is therefore envisioned that the *efficiency cliff* of nanoscale optoelectronic devices can be potentially mitigated by developing semiconducting heterostructures in the deep-nano regime. To date, however, the controlled synthesis and optoelectronic properties of such ultrasmall InGaN nanostructures have remained largely unexplored.

Here, we show that the challenges associated with conventional InGaN nanowires can be fundamentally addressed by developing InGaN micro-network nanostructures in the deep-nano regime. We report on the molecular beam epitaxy (MBE) of InGaN micro-networks grown directly on Si wafer, which can exhibit lateral dimensions as small as 2–5 nm. Detailed structural characterization shows that the self-assembled micro-networks are monocrystalline, despite the complex nanostructures. By controlling the growth conditions, the emission wavelengths can be tuned in the entire visible spectrum. For InGaN micro-network nanostructures emitting in the green wavelength, the emission intensity is nearly two orders of magnitude stronger than conventional InGaN nanowire arrays, due to the significantly reduced defect formation and enhanced exciton oscillator strength. Detailed time-resolved photoluminescence (TRPL) spectroscopy shows that the carrier lifetime is ≈ 6 ns at room temperature. The surface recombination velocity is estimated to be ≈ 150 cm s⁻¹, which is nearly one to two orders of magnitude lower than conventional InGaN nanowire or epilayer structures.^[11] This study provides a new generation of nanostructures that are relevant for high efficiency optoelectronic devices in the deep visible.

2. Results and Discussion

In this study, Ga(In)N micro-network nanostructures were grown on Si substrate utilizing a Veeco Gen II MBE system equipped with a radio-frequency plasma-assisted nitrogen source (see the Experimental Section). Previous studies have shown that, when grown under nitrogen-rich conditions, Ga(In)N nanowires can be readily formed on Si wafer, which are promoted by the initial nucleation of GaN islands on the substrate and their preferential growth along the *c*-axis driven by energy minimization.^[12] Different from conventional nanowire epitaxy, we have employed an ultrathin (approximately sub-nanometer to a few nanometer) AlN buffer layer, schematically shown in **Figure 2a**, to precisely control the formation of crystalline GaN micro-network nanostructures with lateral dimensions in the deep-nano regime, i.e., nearly one order of magnitude reduction compared to conventional nanowires grown by MBE.

AlN buffer layer has been commonly used for the epitaxy of III-nitrides on Si wafer,^[13] but few studies have paid attention to the effect of the initial AlN nucleation on the subsequent growth and epitaxy process. In this study, the thickness of AlN layer was varied from sub-nm to ≈ 8 nm. Due to the large lattice mismatch ($\approx 19\%$), the epitaxy of a thin AlN layer on Si(111) is described by the Volmer-Weber growth mode,^[14] which is characterized by the presence of nanoscale AlN islands, instead of smooth epilayers, on Si substrate. In addition, due to the small Al adatom migration length, these islands are connected, with the presence of extensive voids, forming a nanoscale micro-network-like structure on Si substrate. The atomic force microscopy image of an AlN micro-network structure formed on Si wafer is shown in Figure S1 in the Supporting Information. It is found that the micro-network of AlN islands plays a critical role on the subsequent epitaxy of GaN nanostructures. Impinging Ga adatoms migrate through the opening voids. Different from nanowire epitaxy, however, the nucleation sites of GaN are predetermined by AlN island micro-networks. The nanoscale AlN islands serve as the nucleation sites and promote the coherent epitaxy of GaN, whereas no epitaxy takes place in the opening voids, thereby leading to the formation of unique GaN micro-network nanostructures, schematically shown in Figure 2a. The crystalline AlN island micro-networks further promote the formation of single crystalline InGaN micro-network nanostructures, to be described next.

Schematically shown in Figure 2b–d are scanning electron microscopy (SEM) images of GaN nanostructures grown on Si with the use of various AlN buffer layers under otherwise identical conditions (see the Experimental Section). Shown in Figure 2b, without the use of any AlN buffer layer, conventional GaN nanowire arrays are formed directly on Si wafer, which have diameters ≈ 100 nm and are consistent with previous studies. The introduction of a thin (≈ 1 monolayer) AlN buffer layer, however, leads to the mixture of GaN nanowires and micro-networks. The evolution from nanowires to micro-network nanostructures can be clearly observed with gradual increase of the AlN buffer layer thickness. Further increase of the AlN layer thickness suppresses the formation of nanowires and results in GaN micro-network nanostructures. It is also observed that the AlN buffer layer plays a critical role on the morphology and dimension of GaN micro-networks.

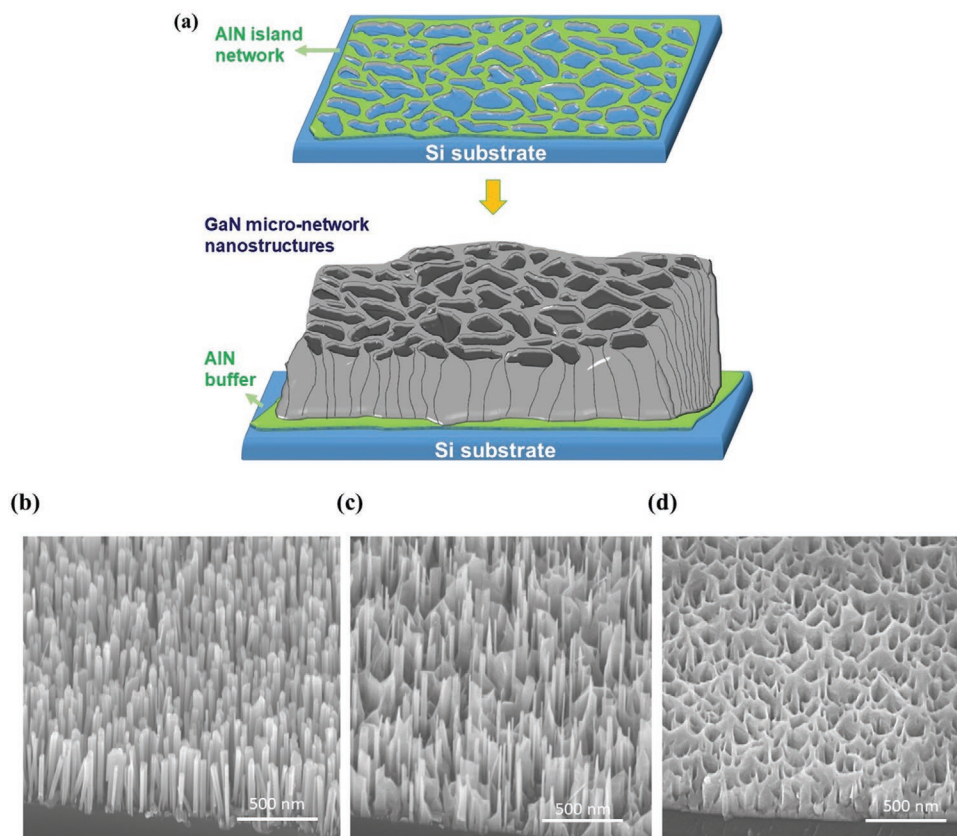


Figure 2. a) Schematic representation GaN micro-network nanostructure grown on Si substrate with AlN buffer layer. b–d) SEM images of GaN nanostructures grown on Si. b) Nanowire arrays are formed on Si in the absence of any AlN buffer layer. c) A mixture of nanowires and micro-network nanostructures are formed on Si with the use of ≈ 1 ML thick AlN buffer layer. d) Formation of GaN micro-network nanostructures on Si with the use of ≈ 8 nm thick AlN buffer layer.

With increasing AlN buffer layer thickness, there is a gradual decrease of the lateral widths of the micro-network structures to as small as ≈ 5 nm. However, further increasing AlN buffer layer thicknesses beyond 5–10 nm leads to the formation of micro-network structures with larger lateral widths and eventual coalescence. The impact of the AlN buffer layer on the initial as well as the complete growth morphology of GaN nanostructures is also depicted in Figures S2 and S3 in the Supporting Information. We have further investigated the effect of growth parameters on the formation and properties of GaN micro-network nanostructures on an AlN buffer layer with a nominal thickness of ≈ 5 nm. It is observed that the lateral widths of micro-network nanostructures show a decreasing trend with increasing N_2 flow rate and/or increasing growth temperature (see Figures S4 and S5, Supporting Information).

The GaN micro-network nanostructures were then utilized as a template for the epitaxy of InGaN nanostructures. N-rich growth conditions were used to promote the epitaxy of InGaN preferentially along the *c*-axis while suppressing the lateral growth (see the Experimental Section). Therefore, InGaN micro-network nanostructures can be readily obtained, shown in Figure 3a,b. Based on the SEM image analysis, it is observed that the average pore size of the structure is $\approx 0.01 \mu\text{m}^{-1}$ with a range of circularity averaging 0.63 and the micro-network lateral

dimension averages at 47.18 nm. The details for the distribution for these parameters are presented in Figure S6a–c in the Supporting Information. Electron microscopy characterization of the InGaN micro-network nanostructure reveals successful large-scale growth of an In-rich InGaN structure with no phase segregation and high crystallinity. The epitaxial growth of an In-rich InGaN segment on top of a bottom GaN layer is further confirmed through STEM imaging and simultaneous chemical mapping of the micro-network nanostructure (Figure 3c and Figure S7, Supporting Information). Indium distribution in the InGaN segment is unconfined and homogeneous, which suggests large-scale incorporation of In-rich crystal across the entire micro-network nanostructure.

As indicated by the sharp diffraction peaks in selected area electron diffraction (SAED) patterns (Figure 3d), the InGaN micro-network nanostructures are single crystal and share a common crystallographic axis. The stark crystallinity of the InGaN micro-network defies initial expectations from the specimen's complex mesoscale morphology. Single crystallinity is maintained across micrometers of material, as shown by the circular aperture selecting the entire micro-network nanostructure in cross-section. Across $\approx 1.75 \mu\text{m}$ of the micro-network laterally, there is only $<0.5^\circ$ rotation of the crystal axis. Crystallinity of the InGaN structure is further verified at atomic resolution with high-angle annular dark field (HAADF) STEM.

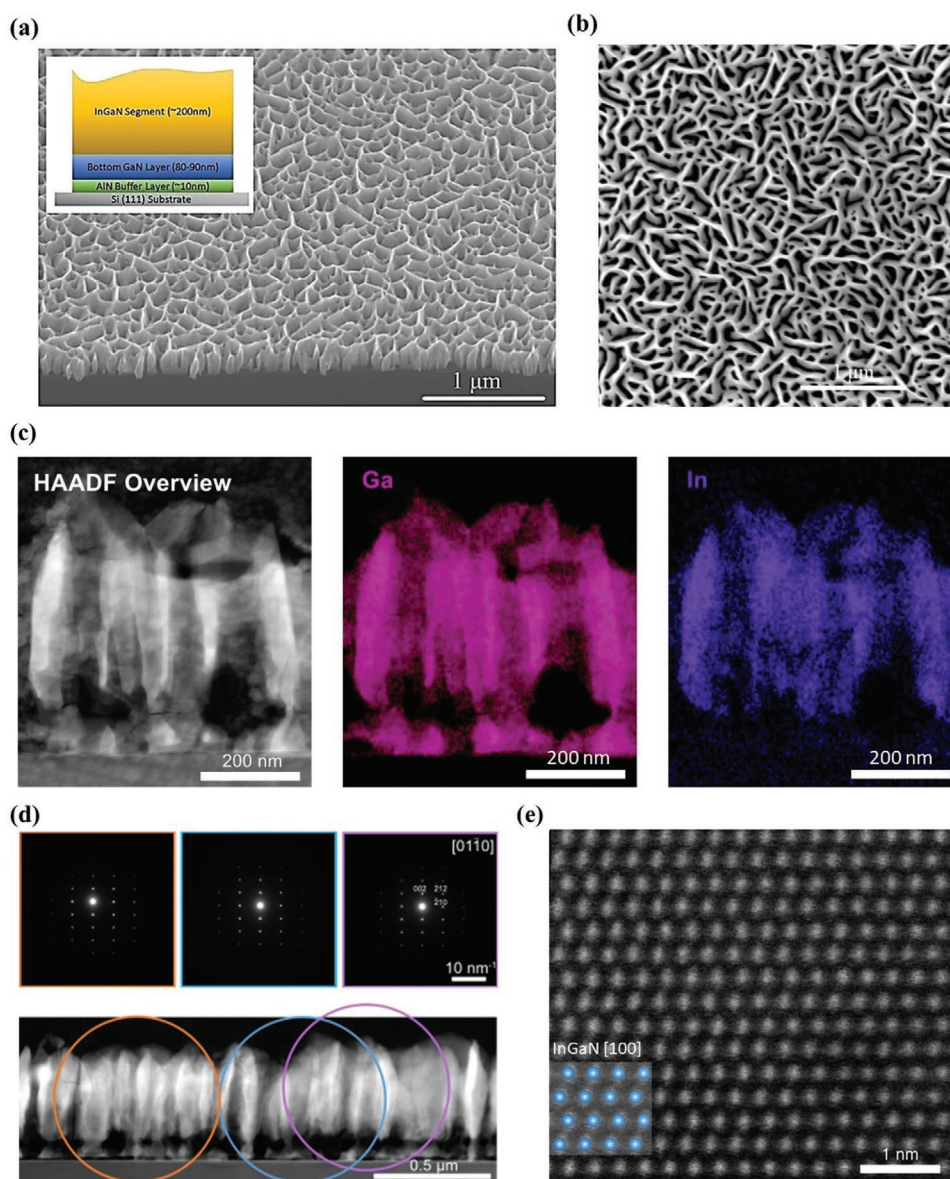


Figure 3. a) SEM image of as-grown InGaN micro-network nanostructures on Si (111) substrate at 45° tilt angle. Inset: Schematic of the layer structure. b) Top view SEM image of as-grown InGaN micro-network nanostructures. c) High-angle annular dark field (HAADF) STEM image of cross-sectional InGaN micro-network nanostructures with energy-dispersive X-ray (EDS) elemental mapping of Ga and In atoms. d) Selected area electron diffraction (SAED) across $\approx 2.5 \mu\text{m}$ of micro-network nanostructure in cross-section. Imaging regions corresponding to each SAED pattern are marked by circular apertures with matching colors. Single-crystallinity is maintained over the entire range ($\approx 2.5 \mu\text{m}$) with only 0.5° crystal rotation over a distance of $1.75 \mu\text{m}$. e) Atomic resolution HAADF-STEM confirms that the specimen is highly crystalline and consistent with the InGaN [100] lattice plane.

The atomic structure in Figure 3e matches that of the [100] lattice plane of InGaN crystal. The unique single crystalline nature of such complex nanostructure arrays is directly related to the coherent epitaxy of GaN on single crystalline AlN island micro-networks. From our atomic resolution HAADF STEM images, there are no discernible dislocations in the specimen over a $15 \text{ nm} \times 15 \text{ nm}$ range; however, dislocations could exist beyond the range indicated. The micro-network lateral widths vary from as small as a few nanometers to tens of nanometer, while the height is $\approx 200 \text{ nm}$. The effects of growth parameters on the formation and properties of InGaN micro-network

nanostructures were further studied in detail and described in Figure S8a–c in the Supporting Information.

InGaN micro-network nanostructures grown on Si can exhibit tunable emission across nearly the entire visible spectrum. Shown in Figure 4a are the normalized photoluminescence spectra measured at room temperature for InGaN micro-networks with various indium incorporation. It is seen that the emission wavelengths can be controllably tuned from blue to the deep visible. Figure 4b shows the room temperature photoluminescence spectra of the InGaN micro-network and that of a conventional InGaN nanowire structure with nearly

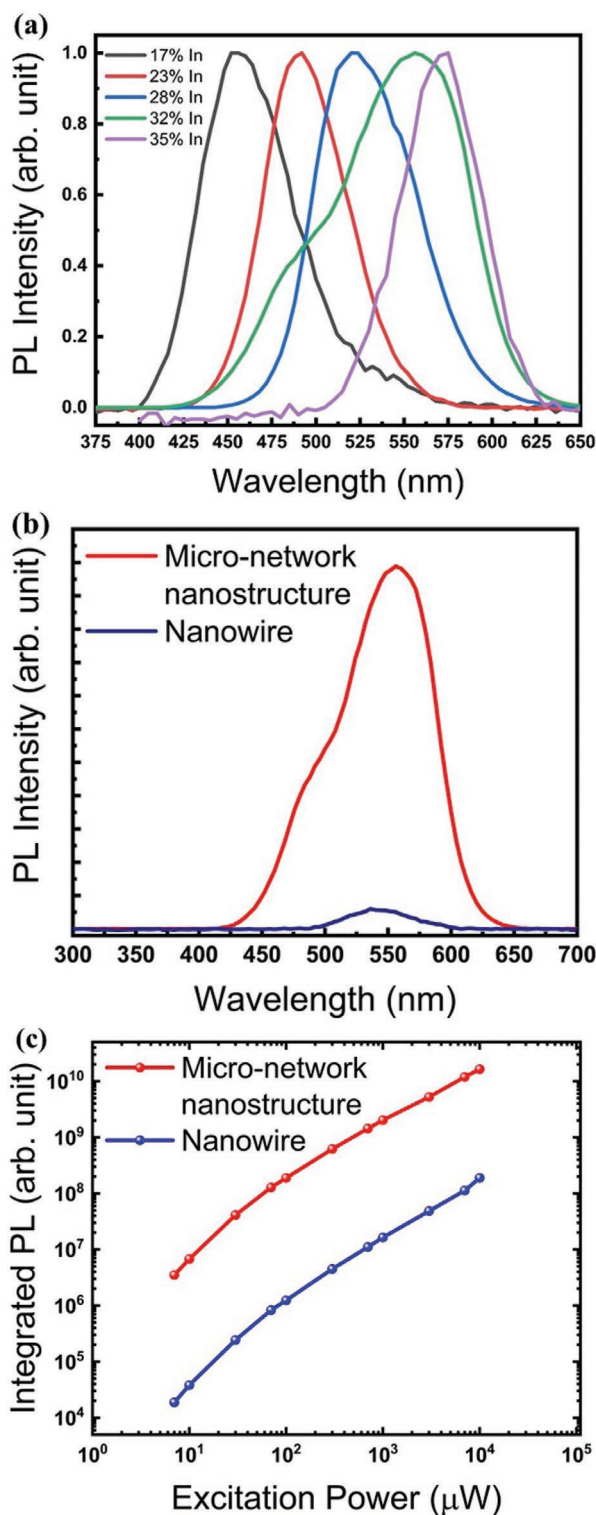
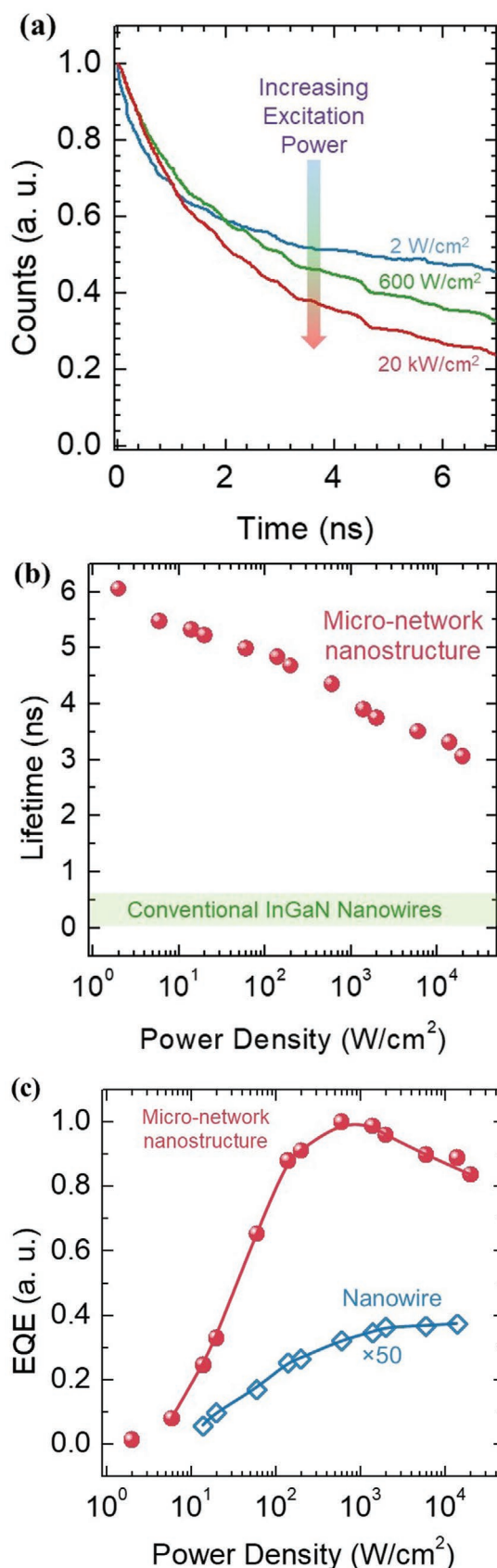


Figure 4. a) Normalized room-temperature photoluminescence (PL) spectra for InGaN micro-network nanostructures, showing tunable emission in the entire visible spectrum. b) Photoluminescence spectra of the InGaN micro-network sample and conventional InGaN nanowire structures with similar surface area, showing nearly two orders of magnitude enhancement of the luminescence emission. c) Variations of the integrated PL intensity with excitation power for InGaN micro-network and nanowire structures measured at room temperature.

identical surface area. It is seen that InGaN micro-network nanostructures exhibit nearly two orders of magnitude enhancement in the luminescence emission. Shown in Figure 4c, the extremely bright photoluminescence emission of InGaN micro-network nanostructures, compared to conventional nanowires, is further confirmed over a broad range of excitation power. It is worth noting that, given their nearly identical surface area, the drastically enhanced luminescence intensity may not be solely explained by variations in the light extraction efficiency. Instead, the ultrabright photoluminescence intensity of the InGaN micro-network nanostructures can be attributed to the significantly reduced nonradiative surface recombination and enhanced exciton oscillator strength in such nanoscale structures. Strain relaxation of InGaN/GaN is most significant in nanostructures with lateral dimensions ≈ 40 nm, or less, as suggested by some recent studies,^[6c,10] thereby leading to drastically reduced nonradiative (surface) recombination. Moreover, efficient strain relaxation leads to significantly reduced piezoelectric polarization fields and therefore enhanced electron–hole wavefunction overlap. As such, the exciton binding energy increases drastically with reducing lateral dimensions of InGaN nanostructures. Exciton binding energy value from 70 meV to larger than 100 meV has been calculated for InGaN nanowall structures with lateral dimensions < 40 nm,^[6c] which is nearly five to ten times larger than that in InGaN bulk. Previous studies further suggested that the exciton oscillator strength of InGaN nanostructures with such small dimensions could be enhanced by nearly 100-fold, compared to quantum well or conventional nanowire structures,^[10] thereby leading to significantly enhanced quantum efficiency and emission intensity.

Optical properties and carrier dynamics of InGaN micro-network nanostructures were further studied utilizing time-resolved femtosecond laser spectroscopy. The samples were excited with the 400 nm output from the second harmonic of a 80 MHz/70 fs Ti:sapphire laser, focused to a spot of 16 μm diameter. The photoluminescence transient was analyzed using a 0.75 m monochromator and a high-speed single photon counter. The photoluminescence transients for the InGaN micro-network sample measured at different excitation power densities from 2 W cm^{-2} to 20 k W cm^{-2} are shown in Figure 5a. The transients were fitted using a standard stretched exponential decay and plotted in Figure 5b, where a relatively long lifetime of over 5 ns was measured for the InGaN micro-network nanostructures at low excitation powers.^[15] Such relatively long carrier lifetime is comparable to that of high quality InGaN quantum well structures despite the large surface area, suggesting that nonradiative surface recombination plays a negligible role in the carrier recombination.^[15c,16] This observation is also consistent with the extremely bright photoluminescence emission measured at room temperature and can be well explained by the robust excitonic emission and reduced Shockley–Read–Hall (SRH) recombination, which would have the dominant effect on carrier lifetime at low carrier densities. At higher excitation, a decrease in lifetime is observed, which can be attributed to the enhanced radiative recombination and, to some extent, higher order carrier loss terms such as Auger recombination and carrier delocalization.^[17] For comparison, significantly shorter carrier lifetime in the range of 0.2–0.5 ns have been commonly measured for conventional InGaN



nanowire arrays, limited by surface recombination, shown in Figure 5b.^[8]

We further performed excitation power dependent measurements on the InGaN micro-network nanostructures as well as some previously reported spontaneous InGaN nanowire samples^[9b] utilizing the same laser source as described above. The photoluminescence signals were analyzed using a 0.75 m monochromator and detected with a UV-enhanced photomultiplier tube (PMT). The relative EQE at different excitation powers is plotted in Figure 5c for both samples. It is seen that the EQE of InGaN micro-network nanostructures is nearly two orders of magnitude higher than that of InGaN nanowire samples, which is consistent with the measurements shown in Figure 4. At higher excitation powers, a clear efficiency droop is observed for the micro-network nanostructures, which is similar to that of conventional high efficiency broad area InGaN light emitters.^[4a] Efficiency droop, however, is not seen for the InGaN nanowire sample, due to the dominant nonradiative SRH recombination. To further analyze the data, the generation rate was estimated for different excitation intensities and described in Figure S9 in the Supporting Information.

Under very low excitation conditions, the carrier lifetime is primarily limited by nonradiative surface recombination for nearly strain and defect-free InGaN nanostructures. If neglecting the contribution of bulk recombination to the carrier lifetime, the nonradiative surface recombination lifetime is estimated ≈ 6 ns for micro-network nanostructures, which is nearly one order of magnitude higher than that of conventional nanowire structures (commonly measured in the range of 0.2–0.5 ns at room temperature). Therefore, an upper bound of the surface recombination velocity (S) can be estimated from the following equation^[18]

$$S = \frac{d}{4\tau_{\text{PL}}} \quad (1)$$

where d is the lateral width of the nanostructures and τ_{PL} is the carrier lifetime determined from the TRPL measurements under low excitation conditions. For the micro-network nanostructures with lateral widths ≈ 30 nm, the surface recombination velocity is calculated to be ≈ 150 cm s⁻¹. For InGaN nanowire samples, based on the commonly measured carrier lifetime ≈ 0.3 ns and nanowire diameters ≈ 100 nm, the surface recombination velocity is estimated to be ≈ 10000 cm s⁻¹. It is seen that the strain relaxed InGaN micro-network nanostructures exhibit a surface recombination velocity that is nearly two orders of magnitude smaller than conventional nanowires. The drastically reduced surface recombination, together with the enhanced electron–hole wavefunction overlap and exciton oscillator strength, can therefore explain the extremely

Figure 5. a) TRPL for InGaN micro-network nanostructures measured at different excitation powers. b) Carrier lifetime versus excitation power density of the InGaN micro-network nanostructures and some previously reported InGaN nanowires at room temperature. c) EQE variation as a function of power density for InGaN micro-network nanostructures and InGaN nanowires, showing nearly two orders of magnitude enhancement of luminescence emission efficiency of micro-network nanostructures, compared to conventional nanowires.

bright luminescence emission of InGaN micro-network nanostructures.

3. Conclusion

In summary, we have performed a detailed study of the epitaxy and characterization of InGaN structures in the deep-nano regime, with lateral dimensions as small as a few nm. These strain-relaxed nanostructures can exhibit drastically reduced defect formation, negligible nonradiative surface recombination as well as significantly enhanced exciton oscillator strength. Compared to conventional nanowire structures with similar surface area, the surface recombination velocity of such deep-nano structures is reduced by nearly two orders of magnitude, which is evidenced by the extremely bright luminescence emission as well as the long carrier lifetime measured at room temperature. This study provides a new direction for the design and development of next generation semiconducting nanostructures to break the efficiency bottleneck of nanoscale optoelectronic devices.

4. Experimental Section

MBE Growth: In this work, the epitaxy of micro-network nanostructures was performed under nitrogen rich conditions using Veeco Gen II radio-frequency plasma-assisted MBE growth system on Si (111) substrate. The Si substrate was cleaned with acetone and methanol and subsequently dipped into 10% buffered hydrofluoric acid prior to loading to eliminate the native oxides. No external metal catalyst was involved for the growth of the micro-network under the nitrogen-rich conditions. The AlN buffer layer growth conditions include a substrate temperature of 810 °C, Al beam equivalent pressure (BEP) of 2×10^{-8} torr, and N₂ flow rate of 1 sccm. The GaN growth conditions include a substrate temperature 680 °C, Ga BEP of 5×10^{-8} torr, and N₂ flow rate 1.5 sccm. Ga BEP of 5×10^{-8} torr, In BEP of 4.5×10^{-8} torr, and 1.5 sccm nitrogen flow rate were used for the InGaN micro-network layer. The initial thin AlN buffer layer was directly grown on Si (111) substrate for up to 5 min. Then, the bottom GaN layer was grown on top of buffer AlN segment for 1 h. The top InGaN layer was subsequently grown for 2 h on top of the GaN layer.

Electron Microscopy Methods: HAADF-STEM images with simultaneous STEM-EDS spectroscopic mapping, and SAED patterns were obtained on a Thermo Fisher Talos F200X G2 (200 keV, 10.5 mrad). The EDS system is equipped with a windowless setup of four silicon drift detectors (SDDs, active area = 4×30 mm², solid angle = 0.9 srad). Atomic resolution HAADF-STEM images were collected using a JEOL 3100R05 microscope with double Cs aberration corrected STEM (300 keV, 22 mrad). Samples for STEM and EDS measurements were prepared in cross-section by mechanical wedge polishing that provides a large and thin area for analyzing samples in the micro-, nano-, and atomic scale.

Structural and Optical Characterization: A He-Cd 325 nm laser was used as the excitation source for measuring the room-temperature PL of the as-grown InGaN nanostructures. The PL emission was detected using a PMT detector coupled to an SPEX spectrometer. Hitachi SU8000 with an accelerating voltage of 10 kV was used for scanning electron microscopy (SEM) imaging.

Supporting Information

Supporting Information is available from the Wiley Online Library or from the author.

Acknowledgements

This work was supported by the College of Engineering at the University of Michigan.

Conflict of Interest

Some IP related to this work was licensed to NX Fuels, Inc., which was co-founded by Z.M. The University of Michigan and Z.M. have a financial interest in NX Fuels.

Data Availability Statement

The data that support the findings of this study are available from the corresponding author upon reasonable request.

Keywords

excitons, light emitting devices, nanostructures, semiconductors, surface recombination

Received: October 21, 2021

Revised: December 10, 2021

Published online: January 8, 2022

- [1] a) M. S. Kang, C.-H. Lee, J. B. Park, H. Yoo, G.-C. Yi, *Nano Energy* **2012**, *1*, 391; b) C.-H. Lee, Y.-J. Kim, Y. J. Hong, S.-R. Jeon, S. Bae, B. H. Hong, G.-C. Yi, *Adv. Mater.* **2011**, *23*, 4614; c) Y. Wang, H. Sun, *Prog. Quantum. Electron.* **2018**, *60*, 1; d) J. M. P. Almeida, V. Tribuzi, R. D. Fonseca, A. J. G. Otuka, P. H. D. Ferreira, V. R. Mastelaro, P. Brajato, A. C. Hernandez, A. Dev, T. Voss, D. S. Correa, C. R. Mendonca, *Opt. Mater.* **2013**, *35*, 2643; e) K. Yu, J. Chen, *Nanoscale Res. Lett.* **2009**, *4*, 1; f) E. Y. Chen, C. Milleville, J. M. O. Zide, M. F. Doty, J. Zhang, *MRS Energy Sustain.* **2019**, *5*, 1. g) J. Park, H. Ryu, T. Son, S. Yeon, *Appl. Phys. Express* **2012**, *5*, 101201; h) L. Sang, J. Hu, R. Zou, Y. Koide, M. Liao, *Sci. Rep.* **2013**, *3*, 2368; i) P. Fan, U. K. Chettiar, L. Cao, F. Afshinmanesh, N. Engheta, M. L. Brongersma, *Nat. Photonics* **2012**, *6*, 380; j) F.-X. Liang, J.-Z. Wang, Z.-P. Li, L.-B. Luo, *Adv. Opt. Mater.* **2017**, *5*, 1700081; k) D. Saxena, S. Mokkapatil, P. Parkinson, N. Jiang, Q. Gao, H. H. Tan, C. Jagadish, *Nat. Photonics* **2013**, *7*, 963.
- [2] S. Zhang, A. T. Connie, D. A. Laleyan, H. P. T. Nguyen, Q. Wang, J. Song, I. Shih, Z. Mi, *IEEE J. Quantum Electron.* **2014**, *50*, 483.
- [3] a) Y. Narukawa, M. Ichikawa, D. Sanga, M. Sano, T. Mukai, *J. Phys. D: Appl. Phys.* **2010**, *43*, 1; b) Y. Narukawa, J. Narita, T. Sakamoto, T. Yamada, H. Narimatsu, M. Sano, T. Mukai, *Phys. Status Solidi A* **2007**, *204*, 2087.
- [4] a) T. Kohno, Y. Sudo, M. Yamauchi, K. Mitsui, H. Kudo, H. Okagawa, Y. Yamada, *Jpn. J. Appl. Phys.* **2012**, *51*, 072102; b) A. Y. Polyakov, N. B. Smirnov, A. V. Govorkov, H. Amano, S. J. Pearton, I.-H. Lee, Q. Sun, J. Han, S. Y. Karpov, *Appl. Phys. Lett.* **2011**, *98*, c) X. Liu, Y. Wu, Y. Malhotra, Y. Sun, Z. Mi, *Appl. Phys. Lett.* **2020**, *117*, 011104.
- [5] a) S. De, A. Layek, S. Bhattacharya, D. K. Das, A. Kadir, A. Bhattacharya, S. Dhar, A. Chowdhury, *Appl. Phys. Lett.* **2012**, *101*, 121919; b) J. W. Robinson, J. H. Rice, K. H. Lee, J. H. Na, R. A. Taylor, D. G. Hasko, R. A. Oliver, M. J. Kappers, C. J. Humphreys, G. A. D. Briggs, *Appl. Phys. Lett.* **2005**, *86*, 213103; c) J.-H. Ryou, P. D. Yoder, J. Liu, Z. Lochner, H. Kim, S. Choi, H. J. Kim, R. D. Dupuis, *IEEE J. Sel. Top. Quantum Electron.* **2009**, *15*, 1080.

- [6] a) A. E. Romanov, T. J. Baker, S. Nakamura, J. S. Speck, *J. Appl. Phys.* **2006**, *100*, 023522; b) T. Takeuchi, H. Amano, I. Akasaki, *Jpn. J. Appl. Phys.* **2000**, *39*, 413; c) S. Sankaranarayanan, S. Chouksey, P. Saha, V. Pendem, A. Udai, T. Aggarwal, S. Ganguly, D. Saha, *Sci. Rep.* **2018**, *8*, 8404.
- [7] F. Glas, *Phys. Rev. B* **2006**, *74*, 121302.
- [8] a) M. Biswas, R. Kumar, A. Chatterjee, Y. Wu, Z. Mi, P. Bhattacharya, S. K. Pal, S. Chakrabarti, *J. Lumin.* **2020**, *222*, 117123; b) S. Deshpande, T. Frost, L. Yan, S. Jahangir, A. Hazari, X. Liu, J. Mirecki-Millunchick, Z. Mi, P. Bhattacharya, *Nano Lett.* **2015**, *15*, 1647; c) W. Guo, M. Zhang, A. Banerjee, P. Bhattacharya, *Nano Lett.* **2010**, *10*, 3355; d) S. Jahangir, A. Banerjee, P. Bhattacharya, *Phys. Status Solidi C* **2013**, *10*, 812; e) C. Zhao, T. K. Ng, R. T. ElAfandy, A. Prabaswara, G. B. Consiglio, I. A. Ajia, I. S. Roqan, B. Janjua, C. Shen, J. Eid, A. Y. Alyamani, M. M. El-Desouki, B. S. Ooi, *Nano Lett.* **2016**, *16*, 4616.
- [9] a) Y. Zhang, J. Wu, M. Aagesen, H. Liu, *J. Phys. D: Appl. Phys.* **2015**, *48*, 463001; b) S. Zhao, H. P. T. Nguyen, M. G. Kibria, Z. Mi, *Prog. Quantum. Electron.* **2015**, *44*, 14.
- [10] a) Y. Kawakami, A. Kaneta, L. Su, Y. Zhu, K. Okamoto, M. Funato, A. Kikuchi, K. Kishino, *J. Appl. Phys.* **2010**, *107*, 023522; b) L. Zhang, L.-K. Lee, C.-H. Teng, T. A. Hill, P.-C. Ku, H. Deng, *Appl. Phys. Lett.* **2014**, *104*, 051116.
- [11] a) R. Aleksiejūnas, M. Sūdžius, T. Malinauskas, J. Vaitkus, K. Jarašiūnas, S. Sakai, *Appl. Phys. Lett.* **2003**, *83*, 1157; b) J. B. Schlager, K. A. Bertness, P. T. Blanchard, L. H. Robins, A. Roshko, N. A. Sanford, *J. Appl. Phys.* **2008**, *103*, 124309; c) V. Ramesh, A. Kikuchi, K. Kishino, M. Funato, Y. Kawakami, *J. Appl. Phys.* **2010**, *107*, 114303; d) K. A. Bulashevich, S. Y. Karpov, *Phys. Status Solidi RRL* **2016**, *10*, 480; e) M. Boroditsky, I. Gontijo, M. Jackson, R. Vrijen, E. Yablonovitch, T. Krauss, C.-C. Cheng, A. Scherer, R. Bhat, M. Krames, *J. Appl. Phys.* **2000**, *87*, 3497; f) H. Kitagawa, T. Suto, M. Fujita, Y. Tanaka, T. Asano, S. Noda, *Appl. Phys. Express* **2008**, *1*, 032004; g) P. Ščajev, K. Jarašiūnas, S. Okur, Ü. Özgür, H. Morkoç, *J. Appl. Phys.* **2012**, *111*, 023702.
- [12] a) R. Calarco, R. J. Meijers, R. K. Debnath, T. Stoica, E. Sutter, H. Luth, *Nano Lett.* **2007**, *7*, 2248; b) R. K. Debnath, R. Meijers, T. Richter, T. Stoica, R. Calarco, H. Lüth, *Appl. Phys. Lett.* **2007**, *90*, 123117.
- [13] a) Y. Tamura, K. Hane, *Nanoscale Res. Lett.* **2015**, *10*, 460; b) A. Zhong, P. Fan, Y. Zhong, D. Zhang, F. Li, J. Luo, Y. Xie, K. Hane, *Nanoscale Res. Lett.* **2018**, *13*, 1391; c) A. Zhong, K. Hane, *Jpn. J. Appl. Phys.* **2013**, *52*, 08JE13.
- [14] a) M. M. R. Evans, J. C. Glueckstein, J. Nogami, *Phys. Rev. B* **1996**, *53*, 4000; b) C. Friesen, S. C. Seel, C. V. Thompson, *J. Appl. Phys.* **2004**, *95*, 1011; c) V. M. Kaganer, B. Jenichen, R. Shayduk, W. Braun, H. Riechert, *Phys. Rev. Lett.* **2009**, *102*, 016103; d) H. Z. Yu, C. V. Thompson, *Acta Mater.* **2014**, *67*, 189.
- [15] a) A. Aiello, A. Pandey, A. Bhattacharya, J. Gim, X. Liu, D. A. Laleyan, R. Hovden, Z. Mi, P. Bhattacharya, *J. Cryst. Growth* **2019**, *508*, 66; b) A. Aiello, Y. Wu, A. Pandey, P. Wang, W. Lee, D. Bayerl, N. Sanders, Z. Deng, J. Gim, K. Sun, R. Hovden, E. Kioupakis, Z. Mi, P. Bhattacharya, *Nano Lett.* **2019**, *19*, 7852; c) M. Pophristic, F. H. Long, C. Tran, I. T. Ferguson, J. R. F. Karlicek, *Appl. Phys. Lett.* **1998**, *73*, 3550.
- [16] a) M. Pophristic, F. H. Long, C. Tran, I. T. Ferguson, J. R. F. Karlicek, *J. Appl. Phys.* **1999**, *86*, 1114; b) Y. C. Shen, G. O. Mueller, S. Watanabe, N. F. Gardner, A. Munkholm, M. R. Krames, *Appl. Phys. Lett.* **2007**, *91*, 141101.
- [17] a) T. Lin, H. C. Kuo, X. D. Jiang, Z. C. Feng, *Nanoscale Res. Lett.* **2017**, *12*, 137; b) T. Lin, Z. R. Qiu, J.-R. Yang, L. Ding, Y. h. Gao, Z. C. Feng, *Mater. Lett.* **2016**, *173*, 170; c) E. F. Schubert, *Light-Emitting Diodes*, Cambridge University Press, Cambridge, UK **2006**.
- [18] a) C.-C. Chang, C.-Y. Chi, M. Yao, N. Huang, C.-C. Chen, J. Theiss, A. W. Bushmaker, S. LaLumondiere, T.-W. Yeh, M. L. Povinelli, C. Zhou, P. D. Dapkus, S. B. Cronin, *Nano Lett.* **2012**, *12*, 4484; b) Y. Dan, K. Seo, K. Takei, J. H. Meza, A. Javey, K. B. Crozier, *Nano Lett.* **2011**, *11*, 2527; c) A. Higuera-Rodriguez, B. Romeira, S. Birindelli, L. E. Black, E. Smalbrugge, P. J. v. Veldhoven, W. M. M. Kessels, M. K. Smit, A. Fiore, *Nano Lett.* **2017**, *17*, 2627.